JOURNAL OF GEOPHYSICAL RESEARCH: ATMOSPHERES, VOL. 118, 1261–1270, doi:10.1029/2012JD017947, 2013

Changes in the variability of the North Pacific sea surface temperature caused by direct sulfate aerosol forcing in China in a coupled general circulation model

Sang-Wook Yeh,[1] Won-Mo Kim,[2,4] Young Ho Kim,[2] Byung-Kwon Moon,[3] Rokjin J. Park,[4] and Chang-Keun Song[5]

Received 15 April 2012; revised 28 November 2012; accepted 2 November 2012; published 14 February 2013.

[1] We examine the direct effect of anthropogenic sulfate aerosol from China on the sea surface temperature (SST) variability in the North Pacific, especially focusing on the Pacific Decadal Oscillation (PDO) using a coupled general circulation model (CGCM). We conduct two long-term simulations, i.e., the Exp_Asia and the Exp_Asia_2x. Anthropogenic sulfate aerosols are prescribed in China only in the Exp_Asia. The conditions for the Exp_Asia_2x simulation are the same as in the Exp_Asia simulation, except the concentration of the anthropogenic sulfate aerosols in China is two times higher than that of the Exp_Asia simulation. It is found that the spatial structure of the PDO changes slightly despite an increase in the anthropogenic sulfate aerosol in China. In contrast, the temporal structure of the PDO is significantly altered between the two simulations. The variance in the PDO index in the boreal winter (December-January-February) and spring (March-April-May) is enhanced for the Exp_Asia_2x on low-frequency timescales (>10 years) compared to that of the Exp_Asia simulation. Upon further analysis, the results of our study indicate that the change in the PDO index from the Exp_Asia to the Exp_Asia_2x is associated with the change in the mean SST in the Kuroshio-Oyashio Extension (KOE) region through the modification of atmospheric circulation. The change in SST in the KOE region is primarily associated with a wave-like temperature structure forced by the diabatic cooling in the low-level atmosphere in China through the modification of atmospheric circulation, which is caused by an increase in the anthropogenic sulfate aerosols. Therefore, it is possible for the temporal structure of the North Pacific SST variability (i.e., PDO) to be altered through the mean SST change in the North Pacific Ocean caused by an increase in regional sulfate aerosols in China.

Citation: Yeh, S.-W., W.-M. Kim, Y. H. Kim, B.-K. Moon, R. J. Park, and C.-K. Song (2013), Changes in the variability of the North Pacific sea surface temperature caused by direct sulfate aerosol forcing in China in a coupled general circulation model, *J. Geophys. Res. Atmos.*, *118*, 1261–1270, doi:10.1029/2012JD017947.

1. Introduction

[2] As reported in the Intergovernmental Panel on Climate Change (IPCC) Fourth Assessment Report [*Trenberth et al.*, 2007], an increase in anthropogenic greenhouse gases and atmospheric aerosols caused by human activity is recognized as the primary force responsible for climate change over the globe. Among these gases and aerosols, sulfate aerosols cool the Earth directly by increasing the scattering of solar radiation and indirectly by providing condensation nuclei for cloud formation; the latter modifies the microphysics, radiative properties, lifetime, and extent of clouds [*Huang et al.*, 2007a]. A direct effect from scattering alone is the cooling of both the surface and atmosphere and an increase in the Earth's albedo [*Charlson et al.*, 1991; *Schwartz*, 1996; *Huang et al.*, 2007b]. In contrast, indirect effects from an increase in aerosols are an increase in the cloud droplet concentration and a decrease in the cloud drop size, which results in an increase in cloud albedo [*Twomey*, 1974; *Hansen et al.*, 1997].

[3] The sources of sulfate aerosols are anthropogenic, biogenic, and volcanic activities [*Chin and Jacob*, 1996]. Approximately 70% of the global emissions of sulfur to the atmosphere are anthropogenic, and 70% of the anthropogenic

[1]Department of Marine Sciences and Convergent Technology, Hanyang University, ERICA, Korea.
[2]Korea Institute of Ocean Science & Technology, Ansan, Korea.
[3]Division of Science Education/Institute of Fusion Science, Chonbuk National University, Jeonju, Korea.
[4]School of Earth and Environment Sciences, Seoul National University, Seoul, Korea.
[5]Global Environment Research Center, National Institute of Environmental Research, Incheon, Korea.

Corresponding author: S.-W. Yeh, Department of Marine Sciences and Convergent Technology, Hanyang University, ERICA, Korea. (swyeh@hanyang.ac.kr)

2169-897X/13/2012JD017947

sources are concentrated in the United States, Europe, and eastern Asia [*Spiro et al*., 1992; *BenKovitz et al*., 1996]. The concentrations of anthropogenic aerosols are the highest over those regions with high industrial activities and/or biomass burning [*Charlson et al*., 1992; *Kiehl and Briegleb*, 1993; *Penner et al*., 2001; *Ramanathan et al*., 2001; *Menon et al*., 2002]; however, their climate impacts are very complex. It is apparent that anthropogenic aerosols exert a radiative influence on the climate that is comparable to that of greenhouse gases, but opposite in sign. The effects of anthropogenic aerosols on the climate have been studied extensively in the past, with the studies focusing on estimation of the direct and indirect impacts on radiative forcing, surface temperature, cloud radiative properties, and precipitation [*Charlson et al*., 1991; *Haywood et al*., 1997; *Menon et al*., 2002; *Giorgi et al*., 2002; *Andreae et al*., 2004; *Korean et al*., 2004; *Huang et al*., 2007b]. In addition, recent studies have examined how climate-chemistry interactions contribute to change in atmospheric composition and climate forcing in the future [*Isaksen et al*., 2009].

[4] However, a critical uncertainty in assessing the effect of anthropogenic sulfur emission on the climate exists in terms of the spatial and temporal extent of the anthropogenic aerosol. In addition, previous studies have primarily focused on the aforementioned issues in atmospheric chemistry and atmospheric climate variability. To date, a limited number of studies [*Chung and Ramanathan*, 2006; *Evan et al*., 2011] have focused on how anthropogenic aerosol forcing is associated with oceanic variables, such as sea surface temperature (SST), using a long-term period of simulation with the ocean-atmosphere coupled general circulation model (CGCM) [*Shindell et al*., 2008; *Kloster et al*., 2010; *Koch et al*., 2011].

[5] According to previous studies, the total energy consumption in Asia more than doubled between 1980 and 2003, causing rapid growth in Asian emissions including a 119% increase in SO_2 emissions [*Ohara et al*., 2007]. In particular, the emissions in China showed a marked increase during that time period, and the growth in emissions since 2000 has also been extremely high [*Lu et al*., 2010]. This increase in China's emissions is primarily caused by the increase in coal combustion in power plants and industrial sectors. Therefore, we may conclude that the total emission for Asia is strongly influenced by the emissions in China. In addition, the largest increase in SO_2 emission between 2000 and 2030 is expected to occur in China, based on the scenarios used in the ACCENT model comparisons [*Isaksen et al*., 2009; *Stevenson et al*., 2006]. In this paper, we focus on how the increase in anthropogenic sulfur emissions in China affects the North Pacific SST variability, including the Pacific Decadal Oscillation (PDO), which is the most dominant SST variability in the North Pacific, in particular. The fact that the North Pacific is located downstream of China makes it possible for changes in the anthropogenic sulfur emissions to influence the SST variability in the North Pacific. In order to study this phenomenon, we compare two runs: a control run in which the anthropogenic sulfate aerosols are prescribed in China in a CGCM and another run that is the same as the control run except the concentrations of anthropogenic sulfate aerosols in China are doubled. From this point forward, we refer to the former and the latter experiments as the Exp_Asia and the Exp_Asia_2x, respectively.

[6] Detailed descriptions of the model and methodology are provided in section 2. In section 3 we discuss the results based on the two simulations of the CGCM in the Exp_Asia and the Exp_Asia_2x using the CGCM. Concluding remarks are given in section 4.

2. Model and Methodology

[7] We run the Community Climate System Model version 2 (CCSM2) that includes atmospheric, oceanic, sea ice, and land component models mutually linked by means of a coupler [*Kiehl and Gent*, 2004]. The atmospheric component of the CCSM2 is the Community Atmospheric Model version 2.0 (CAM2), which has a T31 horizontal resolution and 26 vertical levels. The ocean component uses the Parallel Ocean Program [*Smith et al*., 1992], which has a horizontal resolution of 3.75° in the zonal direction and 1.2° in the meridional direction. The land and sea ice components of the CCSM2 are the Community Land Model version 2.0 and the Community Sea Ice Model version 4, respectively, which have the same horizontal resolution as the atmospheric and ocean component models. A more detailed description of the CCSM2 can be found in a previous study by *Kiehl and Gent* [2004]. We use the observation SST data that are taken from the extended, reconstructed SST version 3 [ERSST.v3; *Smith et al*., 2008] for a comparison with the model output. The ERSST data have a 2.0° spatial resolution. The period during which all of the data were collected spanned 60 years, from 1950 to 2009. In addition, the linear trends and the climatological seasonal cycle are removed from the observation SST.

[8] In order to focus on the role of the anthropogenic sulfate aerosols in China, we purposely remove from the CAM2 the impacts of the anthropogenic sulfate aerosols in all of the other regions except East Asia. Therefore, in the Exp_Asia simulation, we prescribe the annual mean emission of the anthropogenic sulfate aerosols in China at 2001, which is obtained using the global chemical transport model [*Park et al*., 2004] with the latest gridded anthropogenic SO_2 emissions over the Asian domain (60°E to 158°E and 13°S to 54°N) [*Streets et al*., 2006; *Zhang et al*., 2009]. The inventory was based on the studies by *Streets et al*. [2006], which improved estimations for Chinese industrial sources that had been underestimated in the inventory developed earlier.

[9] Figures 1a and 1b show the annual mean concentrations of the anthropogenic sulfate aerosols prescribed in China in the Exp_Asia and Exp_Asia_2x simulations, respectively. The highest concentration of anthropogenic sulfate aerosols is found in East China in the Exp_Asia simulation. For the Exp_Asia_2x simulation, we doubled the concentration of the anthropogenic sulfate aerosols used in the Exp_Asia. Therefore, the differences between the two runs are solely because of the enhanced concentrations of anthropogenic sulfate aerosols in the Exp_Asia_2x relative to the Exp_Asia simulation. In this study, we conducted a simulation for 550 years in Exp_Asia. In Exp_Asia_2x, the concentration of anthropogenic sulfate aerosols gradually increases in the simulation period of 120 years until it reaches 2 times as much as that in Exp_Asia, and then we spin up the model in the simulation period of 80 years. Therefore, Exp_Asia_2x has been run for 400 years and all of the analysis shown here is based

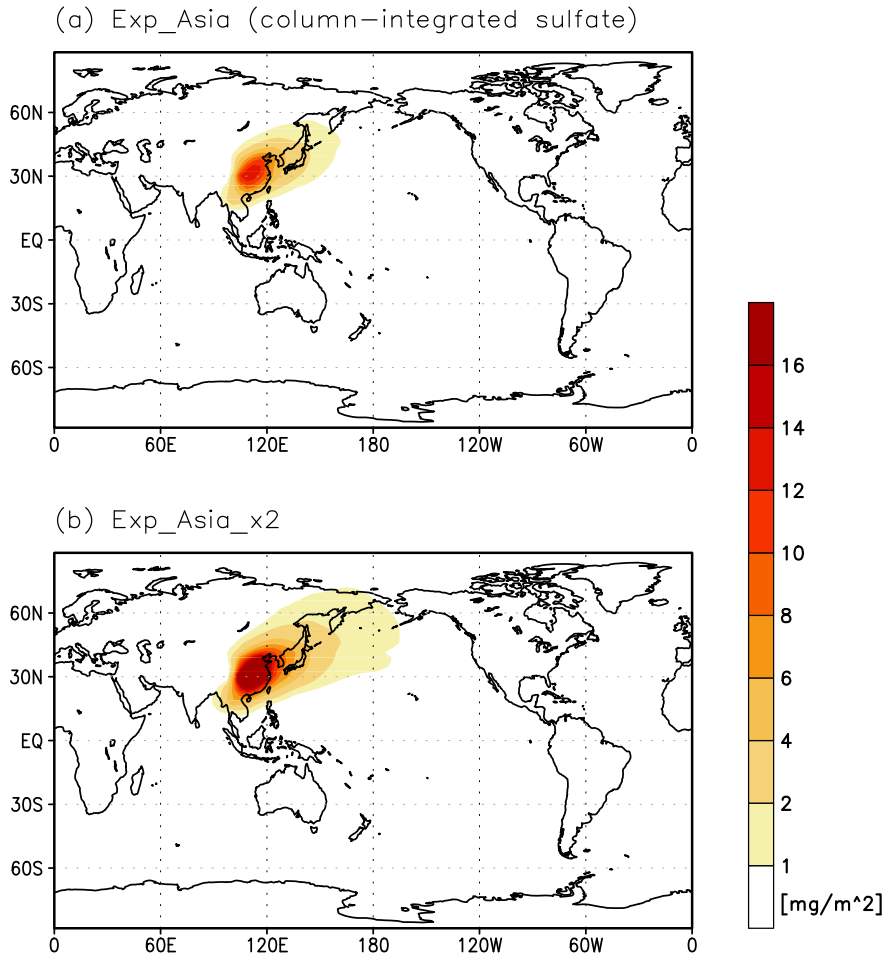

Figure 1. Annual mean concentration of the column-integrated anthropogenic sulfate aerosols prescribed in the (a) Exp_Asia run and the (b) Exp_Asia_2x run. Unit is mg/m^2.

on the data for the last 200 years, which has been compared with Exp_Asia. Note that aerosol indirect effects are not included in both simulations.

[10] Figure 2a shows the difference in the downwelling shortwave flux at surface between the Exp_Asia_2x and the Exp_Asia (Exp_Asia_2x minus Exp_Asia) results during the entire simulation period. A large reduction in the surface shortwave flux, which is mainly caused by a direct effect of the anthropogenic sulfate aerosols in the CGCM, is found in China. The concentration of the anthropogenic sulfate aerosols in China in the Exp_Asia_2x simulation is twice the concentration in the Exp_Asia simulation, as shown in Figure 1. These results indicate that the direct effect of anthropogenic sulfate aerosols is reasonably simulated using Exp_Asia_2x. In contrast, Figure 2b is the same as Figure 2a except for the difference in radiative forcings at the surface, i.e., the summation of net shortwave flux and net longwave flux, between the two simulations during the entire simulation period. One can see that the difference in radiative forcings at the surface in China is mostly caused by downwelling shortwave flux between the two simulations. In contrast, there are also regions where the difference in radiative forcings at the surface is significant in the downstream region of the North Pacific including the Yellow Sea. This might be associated with changes in atmospheric circulation, which will be discussed in section 3.

3. Results

[11] First, we determine the spatial structure of the PDO in the observation data (Figure 3a) and the simulation data from the Exp_Asia (Figure 3b) and Exp_Asia_2x (Figure 3c) simulations, which are obtained using the leading empirical orthogonal function (EOF). The spatial structure accounts for 24%, 21%, and 23% of the total variance in the SST anomalies in the observation, Exp_Asia, and Exp_Asia_2x data, respectively. The geographical pattern of the models' PDOs for the Exp_Asia and Exp_Asia_2x simulations has both some similarities to and some differences from that of the observation data. The overall spatial manifestations of the positive phase of the simulated PDOs in both runs (Figures 3b and 3c) are characterized by cool temperatures in the western and central North Pacific with an elliptical shape and are accompanied by anomalously warm temperatures to the east, north, and south. These results seem to be in agreement with the observation data results (Figure 3a). However, the details of PDO structure in both simulations have some differences from those in the observation. For example, the center of the simulated PDO is shifted to the

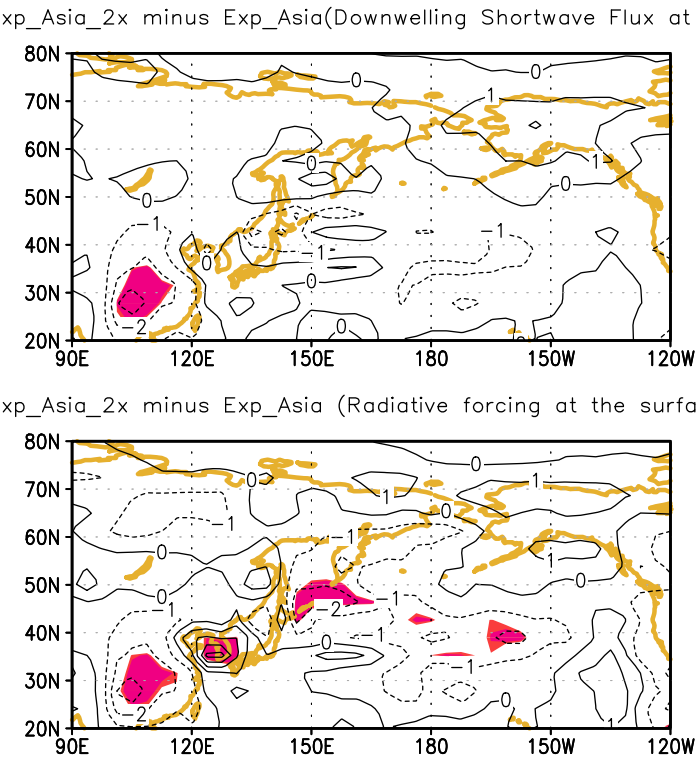

Figure 2. (a) Spatial difference between the Exp_Asia_2x run and the Exp_Asia run (Exp_Asia_2x minus Exp_Asia) in the downwelling shortwave radiation flux at the surface during the entire simulation period. (b) is the same as (a) except for the radiative forcing at the surface. Unit is W/m^2. Shading denotes the region where the difference is statistically significant at the 90% confidence level based on the *T*-test.

west in both runs, and its maximum variance is located in the western North Pacific along the Kuroshio-Oyashio Extension (KOE) near 40°N in comparison with the observation data. The PDO in the observation data has its primary maximum in the central North Pacific with a secondary maximum along the KOE [*Deser and Blackmon*, 1995; *Mantua et al.*, 1997; *Nakamura et al.*, 1997; *Schneider and Cornuelle*, 2005; *Kwon and Deser*, 2007]. Note that the pattern correlation between the PDOs (Figures 3b and 3c) simulated in Exp_Asia and Exp_Asia_2x is 0.98, which is statistically significant at the 95% confidence level. We argue that an increase in the anthropogenic sulfur in China has little impact on the spatial pattern of the PDO by directly comparing the simulated PDOs of both runs.

[12] In order to determine the changes in the temporal structure of the PDO, we examine the power spectrum of the PDO index in the Exp_Asia, the Exp_Asia_2x simulations and the observations (Figure 4) based on Tukey's spectral analysis. The PDO index is defined as the principal component time series of the leading EOF in each run. Various timescales of variability from a short period to low-frequency timescales may be found in the PDO indices in both runs and the observation. In addition, the spectral density of the PDO indices in both runs exhibits pronounced decadal variability without a spectral peak, which also can be found in the observations. The PDO index in the Exp_Asia_2x simulation varies significantly on the low-frequency timescales, while the indices in both the Exp_Asia simulation and the observation do not. For instance, the spectral density of a longer period than the 10 year period is significantly higher in Exp_Asia_2x than in Exp_Asia and the observation by as much as 50%.

[13] Interestingly, a similar increase in the spectral density on the low-frequency timescales is also found in the PDO variability during the boreal winter (December-January-February) and spring (March-April-May) (Figures 5a–5f). Figures 5a–5c are the same as Figure 4, except they are for spring. Figures 5d–5f are the same as Figure 4, except they are for winter. First of all, the spectral density of Exp_Asia (Figures 5a and 5d) and the observation (Figures 5c and 5f) is similar in terms of their magnitude during both seasons. In contrast, the spectral density above the decadal (>10 year period) timescales in Exp_Asai_2x is significantly higher (with a spectral peak around 25 years) by as much as 4 times, than the Exp_Asia simulation and the observation in both seasons. It should be noted that the spectral density of the PDO variability during the boreal summer (June-July-August) and fall (September-October-November) does not show a significant difference when compared to that during the winter and spring (not shown here). Overall, these results indicate that an increase in the anthropogenic sulfate aerosols in China tends to change the temporal structure of the PDO on the low-frequency timescales, during the spring and winter in particular.

[14] The spatial structure of the simulated PDOs in both runs is characterized by a maximum variance of the SST anomaly (SSTA) in the KOE region near 40°N, as shown in Figures 3b and 3c. This result indicates that the PDO variability is highly correlated with the SST variability in the KOE region. As expected, the PDO index is highly correlated with the variability of the average SSTA in the KOE region

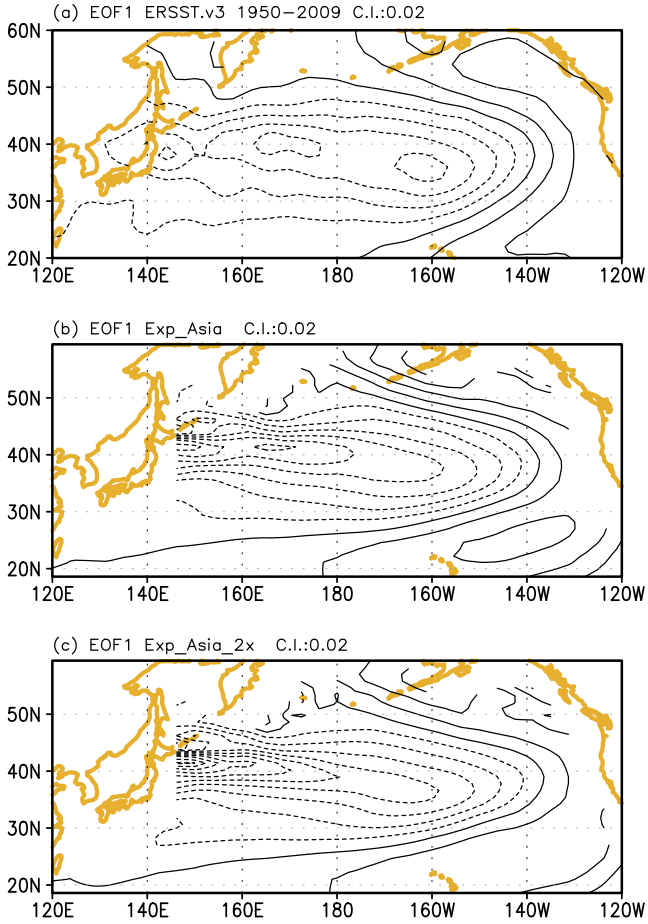

Figure 3. The leading empirical orthogonal function (EOF) in the (a) observation data, (b) the Exp_Asia run, and (c) the Exp_Asia_2x run. Shading denotes positive values. The contour interval is 0.02 and the unit is nondimensional.

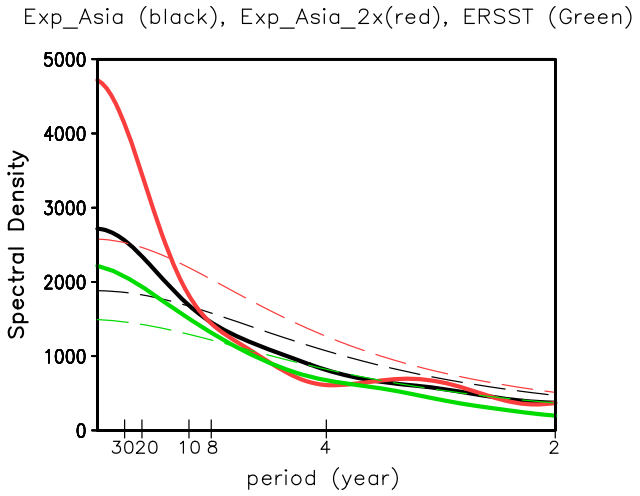

Figure 4. Power spectrum of the PDO index in the Exp_Asia (black), the Exp_Asia_2x (red), and the observation data for the period of 1950-2009 (green). The solid line denotes the power spectra, and the dashed line corresponds to the red-noise power spectra at a 95% confidence level.

(35°N to 45°N, 140°E to 170°E). The simultaneous correlation coefficient is statistically significant at a 99% confidence level during the four seasons in both the Exp_Asia and the Exp_Asia_2x simulations (Table 1). Not surprisingly, the SSTA variability in the KOE region also changed in a similar manner to the PDO index from the Exp_Asia to the Exp_Asia_2x simulations, as shown in Figure 5. In other words, the SSTA variance is greater in the Exp_Asia_2x simulation than the Exp_Asia simulation on the low-frequency timescale during the spring and winter (not shown).

[15] Figures 6a–6d illustrate the differences in the SSTA standard deviations between the Exp_Asia and the Exp_Asia_2x simulations (Exp_Asia_2x minus Exp_Asia) during the four seasons. The SSTA variability is significantly greater in the Exp_Asia_2x simulation than the Exp_Asia simulation, particularly during the spring (Figure 6a) and winter (Figure 6d). This result is consistent with the results shown in Figure 5, which displays the enhanced spectral density of the PDO index during the spring and winter. Therefore, it would be useful to investigate the physical processes associated with the changes in the SSTA variability in the KOE region during spring and winter in order to understand the changes in the temporal structure of the PDO index between the Exp_Asia and the Exp_Asia_2x simulations.

[16] We first examine the differences in the El Niño and Southern Oscillation (ENSO) amplitude during the spring and winter between the two runs (Figures 7a and 7b) in order to examine the effects of SST forcings in the tropical Pacific. There is little difference in the ENSO amplitude between the two runs during both of the seasons. In addition, no change is found in the ENSO frequency between the Exp_Asia_2x ando the Exp_Asia simulations during winter, when the ENSO frequency simulated in the two runs has a strong spectral density on the biennial timescales (not shown). Overall, there are no significant changes in the ENSO properties between the Exp_Asia and the Exp_Asia_2x simulations in terms of amplitude and frequency. Therefore we can conclude that the temporal changes in the PDO index between the Exp_Asia and the Exp_Asia_2x simulations did not originate from the tropics.

[17] We hypothesize that the changes in the mean SST in the North Pacific are responsible for the changes in the temporal structure of the PDO index between the Exp_Asia and the Exp_Asia_2x simulations. We find that a large reduction in the surface shortwave flux in China, which is primarily because of a direct effect of the anthropogenic sulfate aerosols in the CGCM (Figure 2a), is able to change the mean SST in the downstream region of the North Pacific through a wave-like structure of anomalous temperature. Not surprisingly, the difference in radiative forcings at the surface is also characterized by a wave-like structure in the downstream region of the North Pacific (Figure 2b), indicating that changes in atmospheric circulation exist that lead the changes in radiative forcings over the North Pacific. Figure 8a shows the difference in surface mean temperature between the Exp_Asia and the Exp_Asia_2x simulations (Exp_Asia_2x minus Exp_Asia), which is largely consistent with the difference in radiative forcings at the surface in terms of their spatial pattern. An anomalous negative temperature is observed in China where the concentration of the anthropogenic sulfate aerosol in the Exp_Asia_2x simulation is double than in the Exp_Asia simulation (Figure 1).

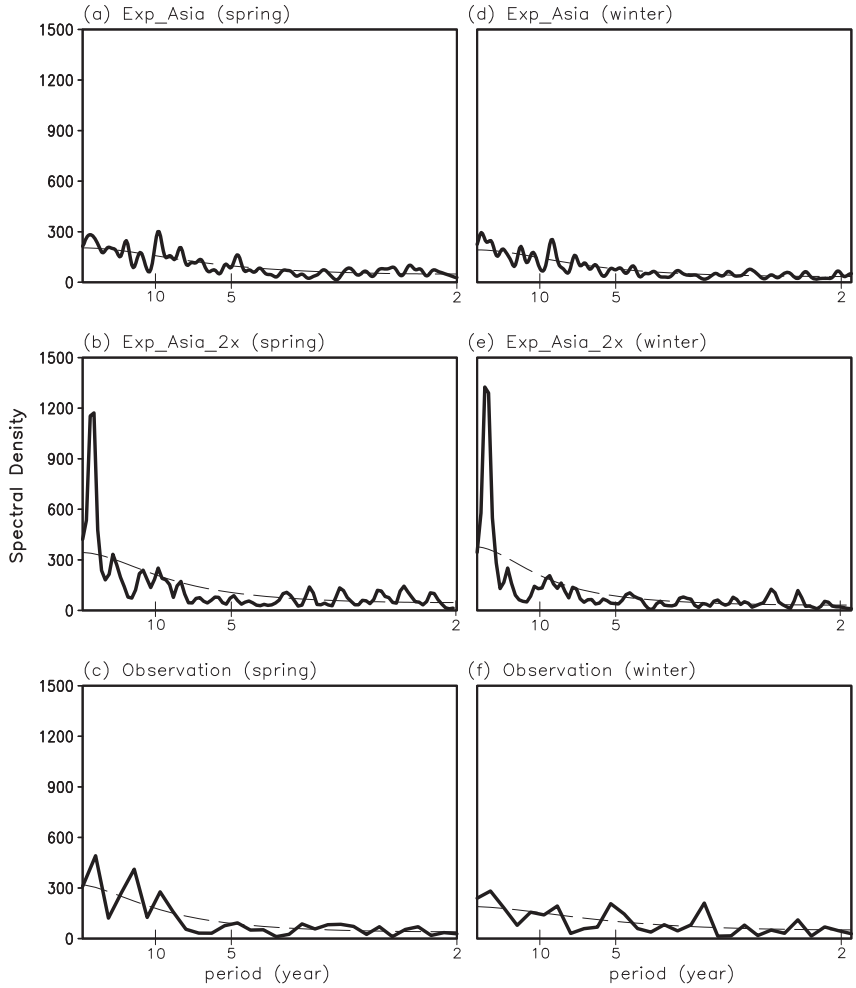

Figure 5. (a–c) The same as in Figure 4 except they are for spring. (d–f) The same as in Figure 4 except they are for winter.

Table 1. Correlation Coefficients Between the PDO Index and the SSTA Variability in the KOE Region During Four Seasons

	Spring	Summer	Fall	Winter
Exp_Asia	-0.89	-0.88	-0.62	-0.82
Exp_Asia_2x	-0.93	-0.89	-0.75	-0.88

In contrast, a significantly warm temperature is found in the Yellow Sea, where positive radiative forcings at the surface are dominant in Exp_Asia_2x compared to Exp_Asia (Figure 2b). In addition, a large difference between the two runs in the mean SST is observed in the KOE region. In other words, a large difference exists in the mean SST in the meridional direction in the KOE region. The wave-like structure of temperature anomalies in the downstream region of the North Pacific may be caused by a cooling in China via a wave-like atmospheric circulation. That is, an increase in the sulfate aerosols in China plays a role in cooling the low-level atmosphere. This cooling causes a change in the mean SST in the downstream region of the North Pacific including the Yellow Sea through the modification of atmospheric circulation over the same region.

[18] To examine more details, we calculate the difference in mean sea level pressure (SLP) and the geopotential height at 500 hPa between the two simulations, respectively, as shown in Figures 8b and 8c. The difference in mean SLP is characterized by a dipole-like structure in the meridional direction. This indicates that the center of the Aleutian Low is shifted to the south from Exp_Asia to Exp_Asia_2x. In addition, the difference in Z500 (Figure 8c) is also characterized by a wave-like structure from China, from the Yellow Sea to the northern North Pacific. We speculate that cooling in China can cause the changes in wave-like atmospheric circulation in the downstream region of North Pacific, resulting in the changes in the mean SST along with the net radiative forcings. In addition, a southward shift of Aleutian low pressure is largely consistent with a southward shift of storm track in the North Pacific, which may lead to an enhanced SSTA variability in the KOE, as shown in Figure 6.

[19] Our results indicate that the meridional SST difference is more significant in the KOE region during the spring and winter than the summer and fall. Figure 9 shows the latitudinal variations of the SST difference, which is zonally averaged in the KOE region (140°E to 165°E) for the spring and winter. In addition, the climatological SST averaged

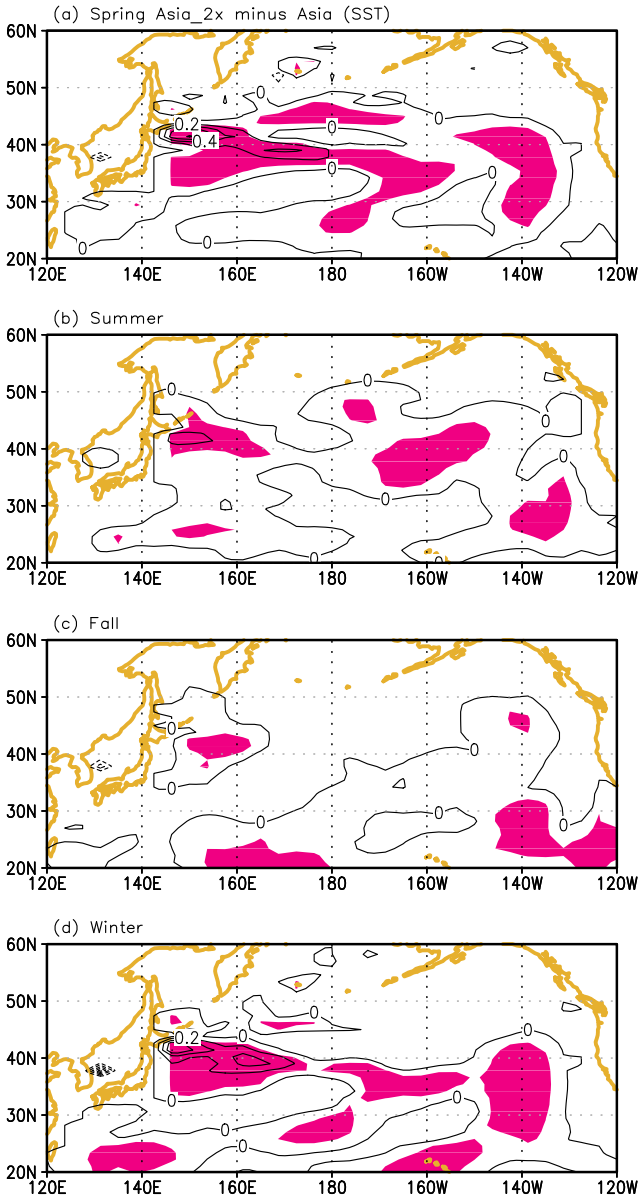

Figure 6. Difference in the SSTA standard deviation between the Exp_Asia and the Exp_Asia_2x (Exp_Asia_2x minus Exp_Asia) simulations during the (a) spring, (b) summer, (c) fall, and (d) winter. The contour interval is 0.2°C. Shading denotes the region where the difference is statistically significant at the 90% confidence level based on the *F*-test.

in the KOE region in the Exp_Asia simulation is also plotted. Figure 9b is the same as Figure 9a except that it shows the variations for the summer and fall. Note that the meridional gradient of climatological SST in the KOE region in spring and winter is stronger than in summer and fall. Furthermore, it is evident that the meridional gradient of the mean SST difference in the KOE region is more significant during the spring and winter (Figure 9a) than the summer and fall (Figure 9b). These results indicate that the meridional SST gradient becomes stronger in the KOE region in the Exp_Asia_2x simulation than the Exp_Asia simulation during the spring and winter, when the change in the

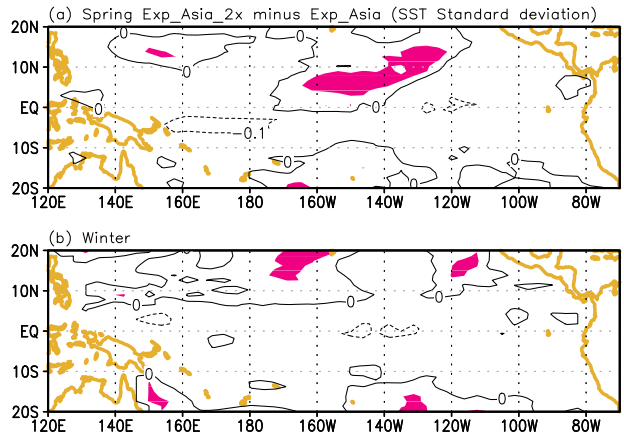

Figure 7. Difference in the SSTA standard deviation during the (a) spring and (b) winter between the Exp_Asia and the Exp_Asia_2x simulations. The contour interval is 0.1°C. Shading denotes the region where the difference is statistically significant at the 90% confidence level based on the *F*-test.

SSTA standard deviation is the most prominent, as shown in Figures 6a and 6d. In addition, one can see that the changes in meridional SST gradient in the KOE region from Exp_Asia to Exp_Asia_2x occur in the region where the meridional gradient of climatological SST in the KOE region is the largest. Therefore, we argue that a wave-like impact of aerosol changes in China may effectively change the strength of the oceanic front via the modification of atmospheric circulation. In contrast, it is difficult to find such differences during the summer and fall (Figure 9b), when the change in the SSTA standard deviation is negligible, as shown in Figures 6b and 6c. Therefore, we can argue that the change in the mean SST plays a role in the change in the SSTA variability in the KOE region, which results in the change in the temporal structure of the PDO index between the Exp_Asia and Exp_Asia_2x simulations.

[20] The enhanced meridional SST gradient in the KOE region that is observed in the Exp_Asia_2x simulation compared to the Exp_Asia simulation may be associated with the enhanced atmospheric eddy activity in the same region, which provides potential energy there. As shown in Figure 8b, in addition, the enhanced atmospheric eddy activity in the KOE region is also consistent with a southward shift of the center of the Aleutian Low from Exp_Asia to Exp_Asia_2x. We could not analyze how the transient eddy influences the SST variability in the KOE region in the Exp_Asia and Exp_Asia_2x simulations, because of lack of data. Even so, we find that the variance difference in the anomalous zonal wind at the lower level (i.e., 850 hPa and 1000 hPa) between the two runs is positive in the KOE region (35°N to 45°N, 140°E to 170°E) during the spring and winter (not shown here). This result indicates that the enhanced SSTA standard deviation in the Exp_Asia_2x simulation might be associated with a strong meridional temperature gradient caused by enhanced atmospheric momentum forcings. We speculate that enhanced atmospheric momentum flux over the KOE region may contribute to the enhanced SSTA variance, particularly on the

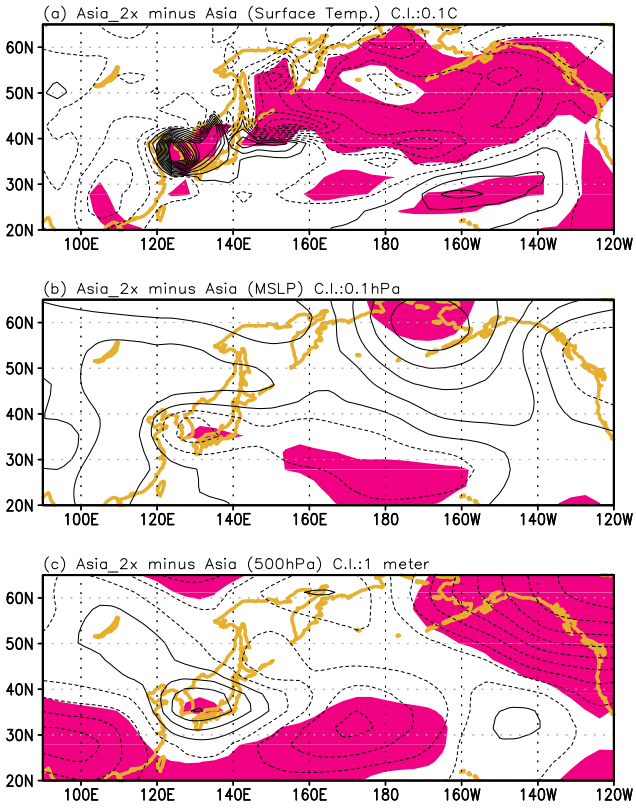

Figure 8. Difference in the climatological surface mean temperature between the Exp_Asia and the Exp_Asia_2x (Exp_Asia_2x minus Exp_Asia) simulations. The dashed line denotes a negative value, and the contour interval is 0.1°C. Shading denotes the region where the difference is statistically significant at the 90% confidence level.

low-frequency timescales, based on the Hasselmann hypothesis [*Hasselmann*, 1976]. In other words, the ocean in the KOE region integrates an enhanced atmospheric momentum forcing between the Exp_Asia and the Exp_Asia_2x simulations and then it transforms a white-noise signal into a red-noise signal, resulting in the enhanced SSTA standard deviation on the low-frequency timescales.

4. Summary and Discussion

[21] Even though aerosols represent a marginal fraction of the atmospheric mass, they play an important role in our climate because they interfere with radiative transfer via the atmosphere. Therefore, the influence of aerosols should be considered for future climate studies. Among the different aerosol species, sulfate aerosols are able to significantly alter the Earth's climate by changing the radiative characteristics of the surface and clouds. In comparison to studies about the effects of anthropogenic aerosols on the climate, less attention has been paid to how anthropogenic sulfate aerosols are associated with climate variability including ocean SST variability. Therefore we focused on how the increase in anthropogenic sulfur emissions in China affects the Pacific Decadal Oscillation by conducting long-term simulations, which included two runs: the Exp_Asia and the Exp_Asia_2x simulations. Anthropogenic sulfate aerosols, which were obtained from a global, three-dimensional, coupled oxidant-aerosol model, were prescribed in China in the Exp_Asia run, and the Exp_Asia was the same as the Exp_Asia_2x run, except that the concentration of anthropogenic sulfate aerosols in China was doubled (Figure 1).

[22] While the spatial structure of the PDO was not significantly changed in spite of an increase in the anthropogenic sulfate aerosols in China, the PDO index in the Exp_Asia_2x simulation had an enhanced variability on low-frequency timescales (>10 years) compared to the Exp_Asia simulation. This was particularly true during the spring and winter seasons. It was found that the temporal variability of the PDO was highly correlated with SST variability in the KOE region. Therefore, the SSTA variance in the KOE region in the Exp_Asia_2x simulation was significantly enhanced during the spring and winter compared to that in the Exp_Asia simulation, which mainly contributes to enhance the PDO

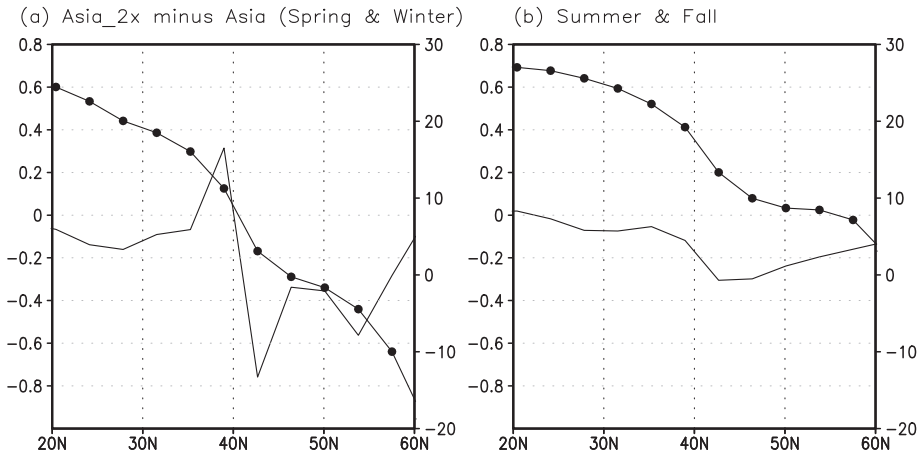

Figure 9. Latitudinal variations in the average climatological SST difference (solid line) between the (a) Exp_Asia and the Exp_Asia_2x (Exp_Asia_2x minus Exp_Asia) simulations in the 140ºE–165ºE range during the spring and winter. (b) The same as (a) except it is for the summer and fall. Note that (b) indicates the magnitude of climatological SST (closed circles) in the 140ºE–165ºE range in Exp_Asia during spring-winter and summer-fall, respectively. Unit is °C.

variability on the low-frequency timescales. By comparing the changes in SSTA variance in the tropical Pacific in the two runs, we could disprove our hypothesis that the temporal changes in the PDO from Exp_Asia to Exp_Asia_2x are from the tropics.

[23] Further analysis indicated that the meridional temperature gradient of the SST around 40°N became stronger in the KOE region, where the meridional temperature of climatological mean SST is the strongest, in the Exp_Asia_2x simulation during the spring and winter than in the Exp_Asia simulation. We argued that a wave-like impact caused by aerosol changes in China may effectively change the strength of the oceanic front via the modification of atmospheric circulation and the changes in mean SST in the North Pacific. Furthermore, it was found that the center of the Aleutian Low is shifted to the south from Exp_Asia to Exp_Asia_2x, which is largely consistent with a southward shift of storm track in the North Pacific. Therefore, we hypothesized that an enhanced momentum flux over the KOE region plays a role in enhancing the SSTA variance on low-frequency timescales between the Exp_Asia and the Exp_Asia_2x simulations. This variance was associated with the changes in the temporal variability of the PDO index between the two runs.

[24] We acknowledge that the results are limited in a single CGCM simulation and that there is a lack of observational evidence to prove the model results. According to recent studies, Asian sulfate has dramatically increased in recent decades [*Isaksen et al*., 2009; *Cofala et al*., 2007; *Stevenson et al*., 2006], therefore, one can argue that this may affect the temporal variability of the PDO index. Despite a short period of observed PDO index in the period 1900 to 2011 (http://jisao.washington.edu/pdo/), we found that the spectral density of the PDO index on the low-frequency timescales is enhanced from the period 1900 to 1949 to the period 1962 to 2011 (not shown here). However, we cannot conclude that such an increase is caused by the increase in Asian sulfate during recent decades because of the short time period of analysis. In contrast, our methodological approach is very simple and idealized, and the CGCM used in this study has a low resolution in the midlatitude ocean. According to a recent study [*Cheon et al*., 2012], the strength of the meridional SST gradient in the KOE region is sensitive to the model resolution. Therefore, some physical processes, as suggested in this study, can be largely dependent on model resolution to some extent. Further study is needed to examine how the changes in SST variability in the North Pacific caused by changes in regional sulfate aerosol forcings are sensitive to the spatial resolution in CGCMs.

[25] **Acknowledgments.** This work was supported by the National Research Foundation of Korea Grant funded by the Korean Government (MEST) (NRF-2009-C1AAA001-2009-0093042). RJP was supported by the Eco Innovation Program of KEITI(ARQ201204015), Korea.

References

Andreae, M. O., D. Rosenfeld, P. Artaxo, A. A. Costa, G. P. Frank, K. M. Longo, and A. F. Silva-Dias (2004), Smoking rain clouds over the Amazon, *Science*, *303*, 1337–1341.

Benkovitz, C. M., M. T. Scholtz, J. Pacyna, L. Tarrason, J. Dignon, E. C. Voldner, P. A. Spiro, J. A. Logan, and T. E. Graedel (1996), Global gridded inventories of anthropogenic emissions of sulfur and nitrogen, *J. Geophys. Res.*, *101*, 29239–29254, doi:10.1029/96JD00126.

Charlson, R. J., J. Langner, H. Rodhe, C. B. Leovy, and S. G. Warren (1991), Perturbation of the northern hemisphere radiative balance by backscattering from anthropogensic sulfate aerosols, *Tellus*, *43AB*, 152–163.

Charlson, R. J., S. E. Schwartz, J. M. Hales, R. D. Cess, J. A. Coakley, J. E. Hansen, and D. J. Hofmann (1992), Sulfate forcing by anthropogenic aerosols, *Science*, *255*, 423–430.

Cheon W.-G., Y. Park, S.-W. Yeh, and B.-M. Kim (2012), Atmospheric impact on the northwestern Pacific under a global warming scenario. *Geophy. Res. Lett.*, *39*, L16709, doi:10.1029/2012GL052364.

Chin, M., and D. J. Jacob (1996), Anthropogenic and natural contributions to tropospheric sulfate: A global model analysis, *J. Geophy. Res.*, *101*(D13), 18691–18699, doi:10.1029/96JD01222.

Chung, C. E., and V. Ramanathan (2006), Weakening of North Indian SST gradients and the monsoon rainfall in India and the Sahel, *J. Climate*, *19*, 2036–2045.

Cofala, J., M. Amann, Z. Klimont, K. Kupiainen, and L. Höglund-Isaksson (2007), Scenarios of global anthropogenic emissions of air pollutants and methane until 2030, *Atmos. Environ.*, *41*, 8486–8499, doi:10.1016/j.atmosenv.2007.07.010.

Deser, C., and M. L. Blackmon (1995), On the relationship between tropical and North Pacific sea surface temperature variations, *J. Climate*, *8*, 1677–1680.

Evan, A. T., J. P. Kossin, C. E. Chung, and V. Ramanathan (2011), Arabian sea tropical cyclones intensified by emission of black carbon and other aerosols, *Nature*, *479*, 94–98.

Giorgi, F., Y. Huang, K. Nishizawa, and C. Fu (2002), Direct radiative forcing and regional climatic effects of anthropogenic aerosols over east Asia: A regional coupled climate-chemistry/aerosol model study, *J. Geophys. Res.*, *107*, 4439, doi:10.1029/2001JD001066.

Hansen, J., M. Sato, and R. Ruedy (1997), Radiative forcing and climate response, *J. Geophys. Res.*, *102*, 6831–6864, doi:10.1029/96JD03436.

Hasselmann, K. (1976), Stochastic climate models, Part I: Theory, *Tellus*, *28*, 473–485.

Haywood, J. M., R. J. Stouffer, R. T. Wetherald, S. Manabe, and V. Ramaswamy (1997), Transient response of a coupled model to estimated changes in greenhouses gas and sulfate concentrations, *Geophys. Res. Lett.*, *24*(11), 1335–1338, doi:10.1029/96GL01163.

Huang, Y., R. E. Dickinson, and W. L. Chameides (2007a), Impact of aerosol indirect effect on surface temperature over East Asia, *Proc. Natl. Acad. Sci. U.S.A.*, *103*, 4371–4376.

Huang, Y., W. L. Chameides, and R. E. Dickinson (2007b), Direct and indirect effects of anthropogenic aerosols on regional precipitation over east Asia, *J. Geophys. Res.*, *112*, D03212, doi:10.1029/2006JD007114.

Isaksen, I. S. A., et al. (2009), Atmospheric composition change: Climate-chemistry interactions, *Atmos. Environ.*, *43*, 5138–5192, doi:10.1016/j.atmosenv.2009.08.003.

Kiehl, J. T., and B. P. Briegleb (1993), The relative role of sulfate aerosols and greenhouses gases in climate forcing, *Science*, *260*, 311–314.

Kiehl, J. T., and P. R. Gent (2004), The community climate system model, version 2, *J. Climate*, *17*, 3666–3682.

Kloster, S., F. Dentener, J. Feichter, F. Raes, U. Lohmann, E. Roeckner, and I. Fischer-Bruns (2010), A GCM study of future climate response to aerosol pollution reductions, *Clim. Dyn.*, *34*, 1177–1194.

Koch, D., et al. (2011), Coupled aerosol-chemistry-climate twentieth century transient model investigation: Trends in short-lived species and climate response, *J. Climate*, *24*, 2693–2714, doi:10.1175/2011JCLI3582.1.

Korean, I., Y. J. Kaufman, L. A. Remer, and J. V. Martins (2004), Measurement of the effects of Amazon smoke on inhibition of cloud formation, *Science*, *303*, 1342–1345.

Kwon, Y. O., and C. Deser (2007), North Pacific decadal variability in the community climate system model version 2, *J. Climate*, *20*, 2416–2433.

Lu, Z., D. G. Streets, Q. Zhang, S. Wang, G. R. Carmichael, Y. F. Cheng, C. Wei, M. Chin, T. Diehl, and Q. Tan (2010), Sulfur dioxide emissions in China and sulfur trends in East Asia since 2000, *Atmos. Chem. Phys.*, *10*, 6311–6331, doi:10.5194/acp-10-6311-2010.

Mantua, N. J., S. R. Hare, Y. Zhang, J. M. Wallace, and R. C. Francis (1997), A Pacific interdecadal climate oscillation with impacts on salmon production, *Bull. Amer. Meteor. Soc.*, *78*, 1069–1079.

Menon, S., J. Hansen, L. Nazarenko, and Y. Luo (2002), Climate effects of black carbon aerosols in China and India, *Science*, *297*, 2250–2253.

Nakamura, H., G. Lin, and T. Yamagata (1997), Decadal climate variability in the North Pacific during the recent decades, *Bull. Amer. Meteor. Soc.*, *78*, 2215–2225.

Ohara, T., H. Akimoto, J. Kurokawa, N. Horii, K. Yamaji, X. Yan, and T. Hayasaka (2007), An Asian emission inventory of anthropogenic emission sources for the period 1980–2020, *Atmos. Chem. Phys.*, *7*, 4419–4444, doi:10.5194/acp-7-4419-2007.

Park, R. J., D. J. Jacob, B. D. Field, R. M. Yantosca, and M. Chin (2004), Natural and transboundary pollution influences on sulfate-nitrate-teammonium aerosols in the United States: Implications for policy, *J. Geophys. Res.*, *109*, D15204, doi:10.1029/2003JD004473.

Penner, J. E., M. Andreae, H. Annegam, L. Barrie, J. Feichter, D. Hegg, R. Leaitch, D. Murphy, J. Ngnga, and G. Pitari (2001), Aerosols, their direct and indirect effects, in Climate Change 2001: The Scientific Basis, edited by J. T. Houghton, et al., pp. 289–348. Cambridge University Press, New York, N. Y.

Ramanathan, V., P. J. Crutzen, J. Kiehl, and D. Rosenfeld (2001), Aerosol, climate and the hydrological cycle, *Science*, *292*, 2119–2124.

Schwartz, S. E. (1996), The whitehouse effect—shortwave radiative forcing of climate by anthropogenic aerosols: An overview, *J. Aerosol Sci.*, *27*, 359–382.

Schneider, N., and B. D. Cornuelle (2005), The forcing of the Pacific Decadal Oscillation, *J. Climate*, *18*, 4355–4373.

Shindell, D. T., H. Levy, II, M. D. Schwarzkopf, L. W. Horowitz, J.-F. Lamarque, and G. Faluvegi (2008), Multimodel projections of climate change from short-lived emissions due to human activities, *J. Geophys. Res.*, *113*, doi:10.1029/2007JD009152.

Smith, R. D., J. K. Dukowicz, and R. C. Malone (1992), Parallel ocean general circulation modeling, *Physica D*, *60*, 38–61.

Smith, T. M., R. W. Reynolds, T. C. Peterson, and J. Lawrimore (2008), Improvements to NOAA's Historical Merged Land-Ocean Surface Temperature Analysis (1880-2006), *J. Climate*, *21*, 2283–2296.

Spiro, P. A., D. A. Jacob, and J. A. Logan (1992), Global inventor of sulfur emission with 1x1 resolution, *J. Geophys. Res.*, *97*, 6023–6036.

Stevenson D. S., et al. (2006), Multimodel ensemble simulations of present-day and near-future tropospheric ozone, *J. Geophys. Res.*, *111*, D08301, doi:10.1029/2005JD006338.

Streets, D. G., Q. Zhang, L. Wang, K. He, J. Hao, Y. Wu, Y. Tang, and G. R. Carmichael (2006), Revisiting China's CO emissions after the Transport and Chemical Evolution over the Pacific (TRACE-P) mission: Synthesis of inventories, atmospheric modeling, and observations. *J. Geophys. Res. Atmos.*, *111*, D14306, doi:10.1029/2006JD007118.

Trenberth, K. E., et al. (2007), Observations: surface and atmospheric climate change, in Climate Change 2007: The Physical Science Basis. Contribution of Working Group I to the Fourth Assessment Report of the Intergovernmental Panel on Climate Change, edited by S. Solomon, et al., Cambridge University Press, Cambridge, UK.

Twomey, S. (1974), Pollution and the planetary albedo, *Atmos. Environ.*, *8*, 1251–1256.

Zhang, Q., et al. (2009), Asian emissions in 2006 for the NASA INTEX-B mission, *Atmos. Chem. Phys.*, *9*, 5131–5153.